Molecular Catalysis 461 (2018) 60–66

Contents lists available at ScienceDirect

Molecular Catalysis

journal homepage: www.elsevier.com/locate/mcat

Ordered mesoporous spinel Co_3O_4 as a promising catalyst for the catalytic oxidation of dibromomethane

Jian Mei[a,b], Jiangkun Xie[a], Zan Qu[a], Yu Ke[a], Xiaofang Hu[a], Naiqiang Yan[a,*]

[a] School of Environmental Science and Engineering, Shanghai Jiao Tong University, 800 Dong Chuan Road, Shanghai, 200240, P. R. China
[b] Jiangsu Key Laboratory of Anaerobic Biotechnology, School of Environment and Civil Engineering, Jiangnan University, Wuxi, 214122, P. R. China

ARTICLE INFO

Keywords:
Ordered mesoporous
Co_3O_4 catalytic oxidation
Dibromomethane

ABSTRACT

The abatement of brominated volatile organic compounds (Br-VOCs) is an urgent task due to their serious harmfulness to human health and the environment. In this work, ordered mesoporous spinel Co_3O_4 was synthesized for the catalytic oxidation of dibromomethane (CH_2Br_2) as a model pollutant for Br-VOCs. The combined results of XRD, BET, and TEM suggested that ordered mesoporous spinel Co_3O_4 was successfully synthesized. Ordered mesoporous spinel Co_3O_4 showed a higher catalytic activity than bulk spinel Co_3O_4. Particularly, Co_3O_4-K showed the highest catalytic activity, and its T_{90} value was only 271 °C. Meanwhile, Co_3O_4-K showed the highest selectivity to CO_2 at low temperature, and a good stability for at least 30 h. The superior catalytic activity was related to their ordered mesoporous channel structures with large specific surface area, high content of active Co^{3+}, and strong redox property. According to the results of product analysis and in situ DRIFT spectra, a reasonable mechanism for CH_2Br_2 oxidation over ordered mesoporous spinel Co_3O_4 was proposed.

1. Introduction

With the implementation of more stringent air pollutants emission standards, more and more people keep their eyes on the emission control of halogenated volatile organic compounds (HVOCs) due to their serious harmfulness to human health, and the environment [1,2]. Brominated volatile organic compounds (Br-VOCs) mainly come from the emission of pesticides, and petrochemicals. Meanwhile, Br-OVCs are also a typical pollutant from the generation of purified terephthalic acid (PTA), and their handling is extremely urgent, and full of challenges due to their difficulty in decomposition [3]. Catalytic oxidation is perceived as an economically viable, and environmentally friendly method to degrade Br-VOCs into CO_2, H_2O, and other harmless substances, making it a potential technology for abating Br-VOCs [4].

Now, the catalysts applied to Br-VOCs oxidation are divided into two parts: precious metals [5], and transition metal oxides [6]. Precious metal generally exhibits a superior activity, but easily produces brominated by-products, and subjects to deactivation due to the adsorption of bromine species. Recently, transition metal oxides have been increasingly researched on Br-VOCs oxidation due to the low cost, and the relatively high resistance to Br poisoning. However, their low catalytic activity is still an intractable problem. Hence, considerable efforts have been devoted to optimizing their performance.

Our previous studies demonstrate that Co-based oxides (e.g., Ti-Co_3O_4, Co_3O_4/CeO_2) have a moderate activity for Br-VOCs oxidation due to their unique redox property, and high concentration of electrophilic oxide species [7]. However, the uses of their active cobalt species for Br-VOCs oxidation are still relatively small. It has been reported that controlling the morphology and structure of Co-based oxides can promote its catalytic activity due to more exposure of active sites [8,9]. Particularly, Co_3O_4 with ordered mesostructured significantly benefit its catalytic activity. Deng et al. compared conventional Co_3O_4 nanoparticles with order mesoporous Co_3O_4 for the degradation of chloramphenicol, and the results suggested that the catalytic performance decreased in the sequence of Co_3O_4-KIT6 > Co_3O_4-SBA15 > nano-Co_3O_4 [10]. Tüysüz et al. believed that order mesoporous Co_3O_4 with high porosity, and specific surface area exhibited better catalytic activity for water oxidation [11]. Song et al. found that mesoporous Co_3O_4, synthesized by an inverse surfactant micelle method, had high catalytic performance for CO oxidation at −60 °C [12]. However, research about ordered mesoporous spinel Co_3O_4 for Br-VOCs oxidation is rare.

In this work, ordered mesoporous spinel Co_3O_4 was synthesized by the nano-replication method using SBA-15, or KIT-6 selected as the template, and bulk spinel Co_3O_4 was synthesized using the co-precipitation method. The physicochemical properties of different Co_3O_4

* Corresponding author.
E-mail address: nqyan@sjtu.edu.cn (N. Yan).

https://doi.org/10.1016/j.mcat.2018.10.001
Received 24 July 2018; Received in revised form 26 September 2018; Accepted 1 October 2018

were characterized by XRD, BET, TEM, XPS, and H_2-TPR techniques. Dibromothane (CH_2Br_2) was explored as the model pollutant for Br-VOCs to evaluate the performance of different Co_3O_4. Product selectivity, and catalyst stability were also investigated. Finally, a reasonable mechanism for CH_2Br_2 oxidation over ordered mesoporous spinel Co_3O_4 was proposed.

2. Experimental section

2.1. Preparation

SBA-15, and KIT-6 were prepared by the hydrothermal method. Tetraethoxysilane (TEOS) was used as the silica source, and P123 ($EO_{20}PO_{70}EO_{20}$) was used as the structure-directing agent. Ordered mesoporous spinel Co_3O_4 was synthesized by the nano-replication method using SBA-15 or KIT-6 as the template. First, 1.0 g of SBA-15 or KIT-6 was added into a $Co(NO_3)_2{\cdot}6H_2O$ ethanol solution (30 mL, 1.0 mol/L). After stirred for 1 h, the ethanol was evaporated at 80 °C, and obtained particles were calcined at 200 °C for 6 h in air. The particles were re-impregnated, and calcined at 500 °C for 3 h in air. SBA-15, and KIT-6 were removed using a NaOH solution (2 mol/L) in 80 °C water bath under magnetic stirring for 16 h. The particles were separated by suction filtration, and then washed with ultrapure water three times. Lastly, the particles were dried at 100 °C for 10 h. The obtained particles were labeled as Co_3O_4-S, and Co_3O_4-K, respectively. Bulk spinel Co_3O_4 (Co_3O_4-B) was synthesized by the co-precipitation method [7,13].

2.2. Characterization

The wide-angle X-ray diffraction pattern (XRD), low-angle XRD pattern, Brunauer-Emmett-Teller (BET) surface area, morphology and microstructure, X-ray photoelectron spectroscopy (XPS), H_2-temperature programmed reduction (H_2-TPR), and in situ DRIFT spectra were monitored on an X-ray diffractometer (Shimadzu, XRD-6100), a SAXS, a N_2 adsorption apparatus (Quantachrome, 2200e), a transmission electron microscopy (TEM, JEOL-2100F), a X-ray photoelectron spectroscope (Shimadzu-Kratos, AXIS UltraDLD), a chemical adsorption apparatus (AutoChem II, 2920), and a Fourier transform infrared spectrometer (FTIR, Nicolet 6700), respectively.

2.3. Activity test

CH_2Br_2 oxidation was conducted in a quartz tube microreactor and the reaction temperature ranged from 150 to 300 °C. The mass of catalyst with 40–60 mesh was generally 80 mg and the total gas flow was 150 mL min^{-1}, resulting in a (GHSV of 112,500 $cm^3\,g^{-1}\,h^{-1}$. The simulated smelting flue gas contained approximately 500 ppm of CH_2Br_2, 10% of O_2, 500 ppm of p-xylene (PX) (when used), 2% of H_2O (when used), and the rest being N_2. The concentration of gaseous CH_2Br_2 was monitored using a gas chromatographer (GC-2010 Plus) equipped with an electron capture detector (ECD). CH_2Br_2 conversion represented the catalytic activity, and it was described as follows:

$$X_{CH_2Br_2} = \frac{C_{in}-C_{out}}{C_{in}} \times 100\% \quad (1)$$

Where C_{in} and C_{out} are the CH_2Br_2 concentrations in the inlet and outlet, respectively.

The products of CH_2Br_2 oxidation were monitored using a GCMS-QP2010. The HBr and Br_2 concentrations were determined using the titration method. First, the gas flow consisting of HBr and Br_2 was entirely absorbed in a KI solution. Then, the Br_2 concentration was determined using the titration method. The bromide ion concentration was determined using an ion chromatography. The CO and CO_2 concentrations were determined using a gas chromatographer (GC-14B). The selectivity to CO, CO_2, Br_2, and HBr can be described as follows,

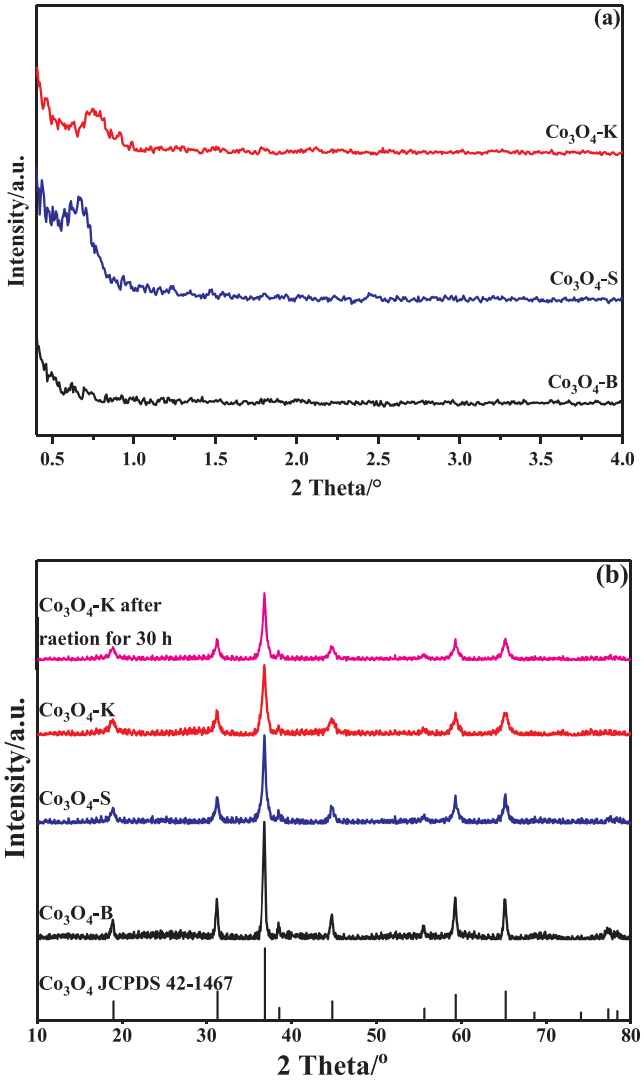

Fig. 1. Low-angle (a), and Wide-angle (b) XRD patterns of different Co_3O_4.

respectively:

$$S_{CO} = \frac{C_{CO}}{C_{in}-C_{out}} \times 100\% \quad (2)$$

$$S_{CO_2} = \frac{C_{CO_2}}{C_{in}-C_{out}} \times 100\% \quad (3)$$

$$S_{Br_2} = \frac{C_{Br_2}}{C_{in}-C_{out}} \times 100\% \quad (4)$$

$$S_{HBr} = \frac{C_{HBr}}{2(C_{in}-C_{out})} \times 100\% \quad (5)$$

Where C_{CO} and C_{CO_2} were the CO and CO_2 concentrations, C_{Br_2} and C_{HBr} were the Br_2 and HBr concentrations, respectively.

3. Results and discussion

3.1. Characterization

The ordered mesoporous structure of different Co_3O_4 is determined by the low-angle XRD patterns, and the results are shown in Fig. 1(a). It is significant to see that the low-angle XRD patterns of both Co_3O_4-S, and Co_3O_4-K displayed a new reflection at 0.5–1.0°, corresponding to the lower symmetry compared with its parent silica. It suggested that

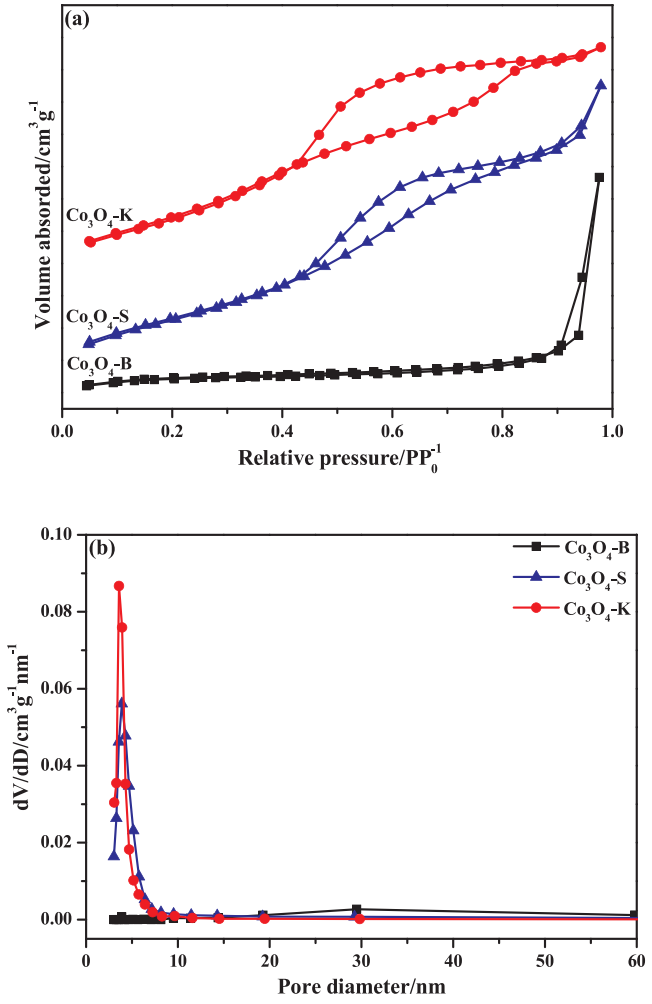

Fig. 2. N_2 adsorption-desorption isotherms (a), and pore size distributions (b) of different Co_3O_4.

ordered mesoporous structure of Co_3O_4 was formed.

The crystal texture of different Co_3O_4 is monitored through the wide-angle XRD patterns, and the results are shown in Fig. 1(b). All the samples showed eight diffraction peaks, which were related to the face-centered cubic spinel Co_3O_4 [14]. However, the intensity of diffraction peaks for Co_3O_4-S, and Co_3O_4-K was weaker than that of Co_3O_4-B, suggesting that ordered mesoporous spinel Co_3O_4 had lower crystallinity and smaller crystallite size. By calculating the Scherrer equation applied for (311) plane, the crystalline sizes of Co_3O_4-B, Co_3O_4-S, and Co_3O_4-K were 28.4, 15.5, and 12.8 nm, respectively.

The N_2 adsorption-desorption isotherms and pore size distributions of different Co_3O_4 are shown in Fig. 2. The N_2 adsorption-desorption isotherms of Co_3O_4-S, and Co_3O_4-K were attributed to type IV with a type H1 hysteresis loop, and their capillary condensation ranges were broad starting at approximately $P/P_0 = 0.45$ and extending almost to $P/P_0 = 0.95$ (Fig. 2(a)), suggesting typically mesoporous structure features. Meanwhile, the hysteresis loop of Co_3O_4-K was larger than that of Co_3O_4-S, suggesting that they had different porous channel structure. The BJH pore size distributions, calculated through the desorption isotherms, showed that Co_3O_4-S, and Co_3O_4-K had a unimodal pore-size distribution centered at 3.9, and 3.6 nm, respectively, which further demonstrates that Co_3O_4-S, and Co_3O_4-K perfectly remained the replica structures of their templates. Textural parameters of different Co_3O_4 estimated by N_2 physisorption are summarized in Table 1. The BET specific surface areas of Co_3O_4-S, and Co_3O_4-K were 86.2, and 94.0 $m^2\ g^{-1}$, respectively, which were larger than that of Co_3O_4-B

Table 1
Textural parameters of different Co_3O_4.

Catalyst	S_{BET} ($m^2\ g^{-1}$)	Average pore diameter (nm)	Average pore volume ($cm^3\ g^{-1}$)	D_{Co3O4} (nm)
Co_3O_4-B	0.2	23.0	0.02	28.4
Co_3O_4-S	86.2	3.9	0.15	15.5
Co_3O_4-K	94.0	3.6	0.12	12.8

D_{Co3O4}:Co_3O_4 crystallite size calculated by Scherrer equation from XRD.

(0.2 $m^2\ g^{-1}$). Similarly, the average pore volumes of Co_3O_4-S, and Co_3O_4-K were also larger than that of Co_3O_4-B. The results suggested that constructing ordered mesoporous structure could significantly improve the BET specific surface area, and average pore volume.

The microscopic morphology and structure information of different Co_3O_4 were obtained through TEM and HRTEM, and the related images are shown in Fig. 3. Co_3O_4-B was composed of single crystals with no pore, and its particle sizes were about 20–30 nm (Fig. 3(a, b)), which was consistent with the result calculated by Scherrer equation from XRD. Co_3O_4-S, and Co_3O_4-K clearly displayed the ordered mesoporous (Fig. 3(c, e)), confirming the good replication of SBA-15, or KIT-6, which was consistent with the results of XRD, and N_2 adsorption-desorption isotherms. Co_3O_4-S was composed of ordered arrangement of nanoparticles with pore size approximately 4–8 nm, while Co_3O_4-K comprised nanoparticles arrayed in a well-ordered framework with pore size varying from 3 to 6 nm. In the HRTEM images, the lattice fringes were clearly visible in all the samples. Co_3O_4-B had the (111) plane with an interplanar spacing of 0.467 nm. Both Co_3O_4-S and Co_3O_4-K had the (111), and (220) planes with interplanar spacing of 0.467, and 0.285 nm, respectively [15]. According to the literatures, the (220) plane was an active surface owing to it mainly comprised Co^{3+}, while the (111) plane was not an active surface due to it was composed of Co^{2+} [16]. Co_3O_4-B only presented the (111) plane, whereas Co_3O_4-S, and Co_3O_4-K exposed the (111), and (220) planes, so Co_3O_4-S, and Co_3O_4-K had the higher catalytic activity.

To ascertain the oxidation states of Co, and O on the surface, XPS was performed, and the related spectra are shown in Fig. 4. All the samples had two main peaks, appeared at 779.0–779.5 eV, and 794.8–795.3 eV (Fig. 4(a)), which was ascribed to Co $2p_{3/2}$, and Co $2p_{1/2}$, respectively. The Co $2p_{3/2}$ XPS spectra could be decomposed into two components, and their binding energy approximately appeared at 778.7–779.4, and 779.8–780.5 eV, which was belong to Co^{3+}, and Co^{2+}, respectively [17]. The Co^{3+}/Co^{2+} ratio was 0.30, 0.37, and 0.39 for Co_3O_4-B, Co_3O_4-S, and Co_3O_4-K, respectively (Table 2). The results suggested that ordered mesoporous spinel Co_3O_4 had more Co^{3+} species, which favored bringing more surface oxygen and promoting gas molecule adsorption (Table 3).

The O 1 s spectra of different Co_3O_4 were resolved into two peaks (Fig. 4(b)). The binding energy appeared at 529.0–529.7 eV were ascribed to the lattice oxygen (O_{lat}), and the binding energy appeared at 530.4–531.2 eV was assigned to surface adsorbed oxygen (O_{ads}) [18]. Co_3O_4-K had the largest O_{ads}/O_{lat} ratio, followed by Co_3O_4-S, and Co_3O_4-B was the least O_{ads}/O_{lat} ratio (Table 2). The results suggested that ordered mesoporous spinel Co_3O_4, especially Co_3O_4-K, had abundant surface active oxygen.

The redox property of the catalyst has a significant impact on catalytic reaction, it can be determined using H_2-TPR experiment, and the results are shown in Fig. 5. Co_3O_4-B had two reduction peaks appeared at 337, and 387 °C, which corresponded to the reduction of Co^{3+} to Co^{2+}, and Co^{2+} to Co^0, respectively [19]. The area of low temperature reduction peak was lower than that of high temperature reduction peak, suggesting that the amount of Co^{2+} was higher than that of Co^{3+}, which was consistent with the XPS results. Co_3O_4-S had three reduction peaks appeared at 305, 366, and 458 °C. The first reduction peak was related to the reduction of Co^{3+} to Co^{2+}, while the latter two reduction

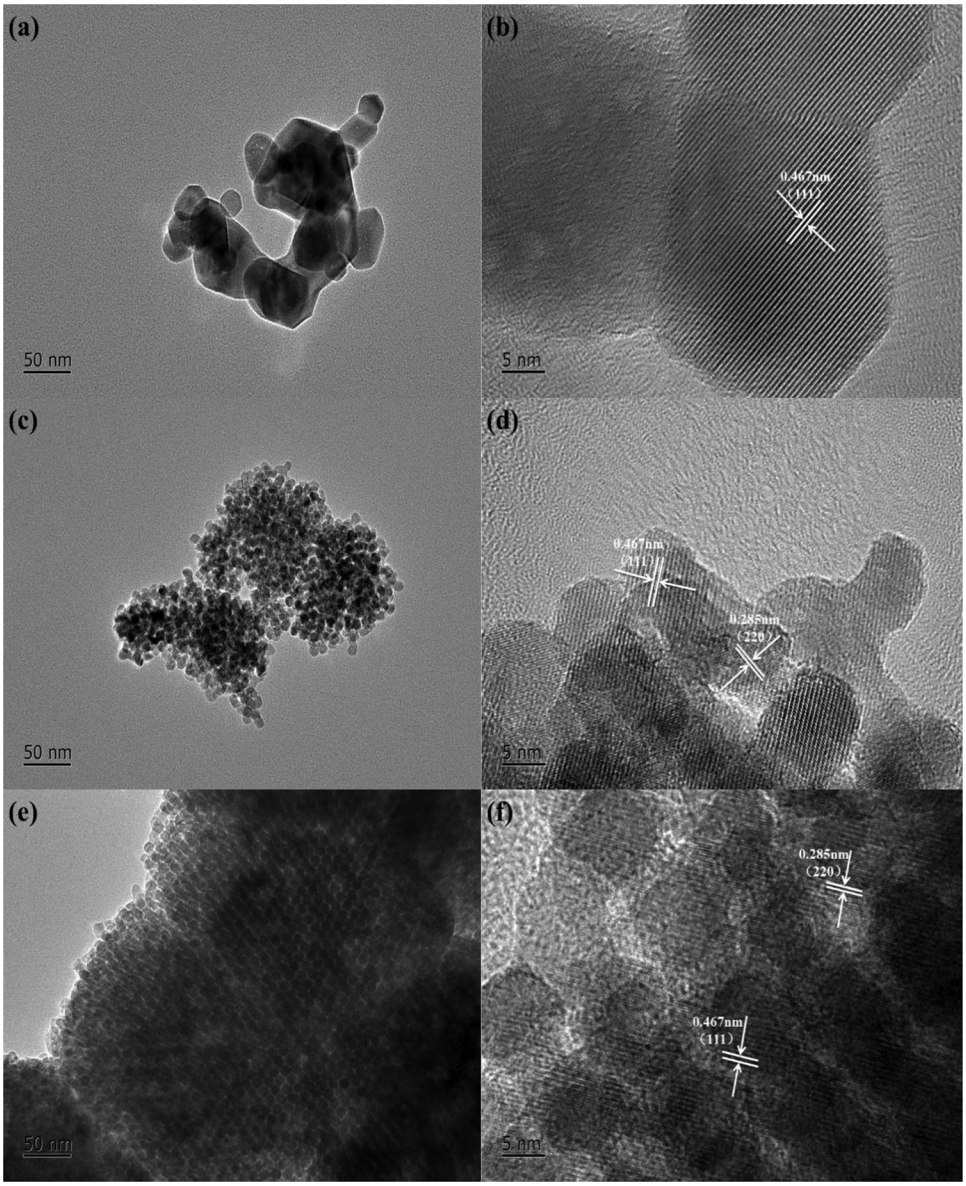

Fig. 3. TEM, and HRTEM images of different Co_3O_4: Co_3O_4-B (a, b), Co_3O_4-S (c, d), and Co_3O_4-K (e, f).

peaks corresponded to the reduction of Co^{2+} to Co^0. The similar result was also observed for Co_3O_4-K, except the reduction peaks shifted to lower temperature. However, the first reduction peak area for Co_3O_4-K was larger than that for Co_3O_4-S, suggesting that Co_3O_4-K had more Co^{3+}. As well known, the more Co^{3+} ions generated the more anionic defects, which was in favor of bringing surface oxygen and promoting the adsorption of reactant molecule. Moreover, Co_3O_4-K had the strongest redox ability owing to the lowest reduction temperature, which was conducive to the catalytic reaction.

3.2. Activity

CH_2Br_2 conversion curves as function of temperature over different Co_3O_4 are shown in Fig. 6. Co_3O_4-B presented the worst oxidation activity, and its T_{90} (the temperature required for 90% conversion) value was approximately 287 °C. Co_3O_4-S had better activity, and its T_{90} value was approximately 274 °C. Co_3O_4-K displayed the highest catalytic activity with a T_{90} value of approximately 271 °C, by reason of the three dimensional porous channels and the large specific surface area of Co_3O_4-K made it easily adsorb CH_2Br_2 molecules. The results suggested that ordered mesoporous spinel Co_3O_4 were in favor of CH_2Br_2 oxidation owing to their unique porous structures.

3.3. Product analysis

It is common knowledge that the ideal products of Br-VOCs oxidation are CO_2, and HBr, or Br_2, however, the current catalysts hardly achieve fully mineralization. Hence, it is essential to analyze the product composition, and product selectivity to the ideal products when developing a novel catalyst. The products over Co_3O_4-B, Co_3O_4-S, and Co_3O_4-K at different temperature were detected by GCMS, and the results are shown in Table S1, S2, and S3. The products were CO, CO_2, HBr, and H_2O at low temperature, and no other Br-containing by-products were monitored. Fig. 7 presents the selectivity to CO, CO_2, HBr, and Br_2 at different temperatures over Co_3O_4-B, Co_3O_4-S, and Co_3O_4-K. For Co_3O_4-B, the selectivity to CO_2, and Br_2 gradually increased with the increase of temperature, while that to CO, and HBr gradually decreased (Fig. 7(a)). Similar phenomena were also observed for Co_3O_4-S, and Co_3O_4-K. The selectivity to CO_2 was approximately 23%, 47%, 61%, and 91% at 150, 175, 200, and 225 °C, respectively, and was 100% above 250 °C. The increase in selectivity to CO_2 was attributed to the deep oxidation of CO at higher temperatures. Additionally, Br_2 was

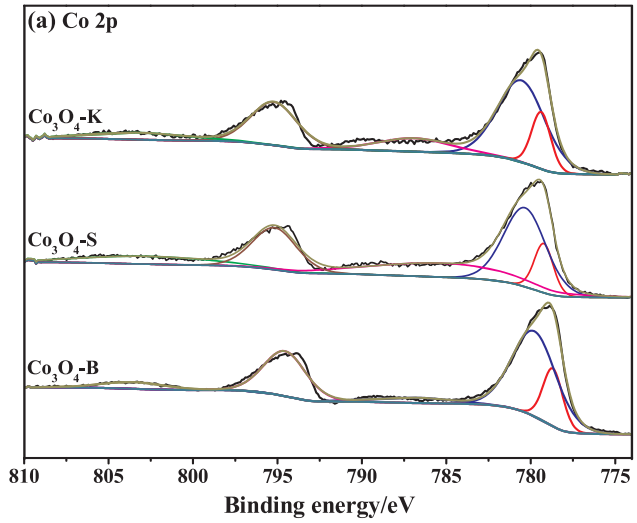

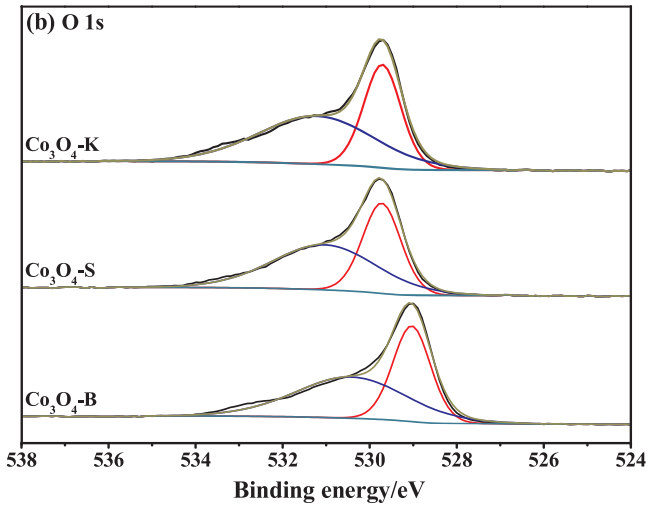

Fig. 4. XPS spectra of Co 2p (a), and O 1s (b) for different Co_3O_4.

Table 2
XPS parameters of different Co_3O_4.

Catalyst	Co^{3+}/Co^{2+}	O_{ads}/O_{lat}
Co_3O_4-B	0.30	1.27
Co_3O_4-S	0.36	1.36
Co_3O_4-K	0.39	1.45

Table 3
Products in outlet at different temperature over Co_3O_4-K.

Temperature (°C)	Detected substances
150	CH_2Br_2, CO, CO_2, HBr, H_2O
175	CH_2Br_2, CO, CO_2, Br_2, HBr, H_2O
200	CH_2Br_2, CO, CO_2, Br_2, HBr, H_2O
225	CH_2Br_2, CO, CO_2, Br_2, HBr, H_2O
250	CH_2Br_2, CO_2, HBr, Br_2, H_2O
275	CH_2Br_2, CO_2, HBr, Br_2, H_2O
300	CO_2, HBr, Br_2, H_2O

formed when the temperature was exceed 175 °C, which was due to the occurrence of Deacon reaction ($4HBr + O_2 \rightarrow 2Br_2 + H_2O$) [20], and the selectivity to Br_2 was 61% at 300 °C. For Co_3O_4-S and Co_3O_4-K, the selectivity to CO_2, and Br_2 were higher than that to Co_3O_4-B. The

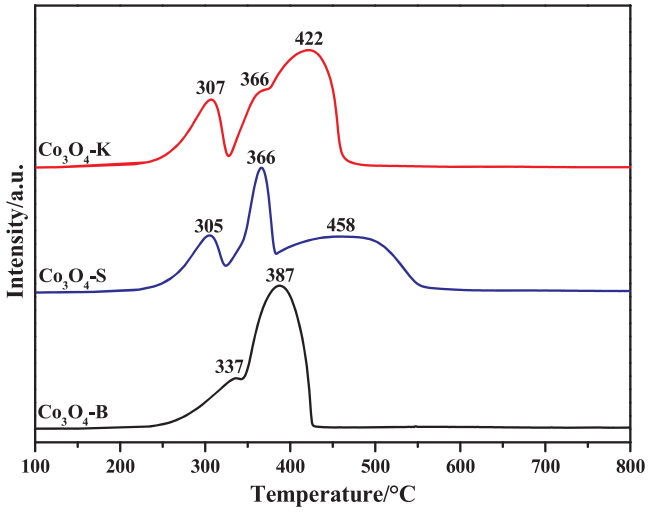

Fig. 5. H_2-TPR profiles of different Co_3O_4.

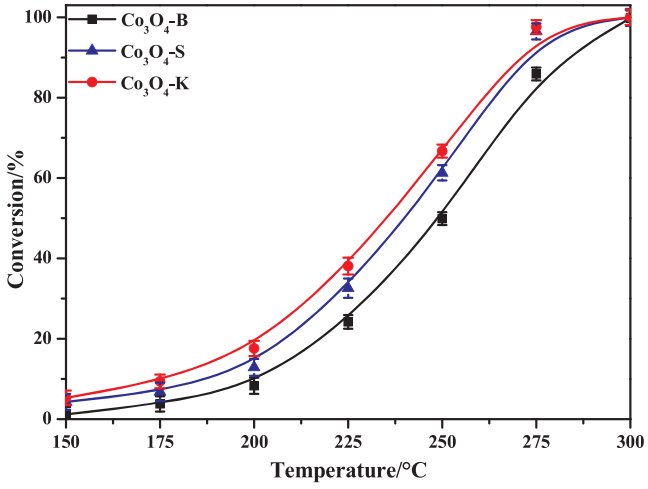

Fig. 6. Conversion curves for CH_2Br_2 oxidation as function of temperature over different Co_3O_4; operating condition: 500 ppm of CH_2Br_2, 10% of O_2, and the rest being N_2; GHSV = 112,500 $cm^3\,g^{-1}\,h^{-1}$.

selectivity to CO_2, and Br_2 were approximately 100%, and 43%, respectively, at 225 °C for Co_3O_4-S (Fig. 7(b)), and approximately 100%, and 65%, respectively, at 225 °C for Co_3O_4-K (Fig. 7(c)). The results suggested that ordered mesoporous spinel Co_3O_4 was beneficial to the deep oxidation of CO to CO_2 and promoted the formation of Br_2.

3.4. The influence of H_2O or PX

Water vapor generally exists in the Br-VOCs-containing industrial exhaust gas, herein, the influence of water vapor on the catalytic activity for CH_2Br_2 oxidation was investigated, and Fig. 8 shows CH_2Br_2 conversion over Co_3O_4-K as a function of temperature in the presence of 2% H_2O. To our surprise, CH_2Br_2 conversion was slightly increased at low temperature in comparison with the result without H_2O, and the T_{10} (the temperature required for 10% conversion) value decreased by approximately 9 °C. The facilitating influence of H_2O over Co_3O_4-K on the catalytic oxidation of CH_2Br_2 can be ascribed to the removal of surface bromine species due to the reverse Deacon reaction: $H_2O + Br^- \leftrightharpoons HBr\uparrow + OH^-$ [21]. However, with the increase of temperature, CH_2Br_2 conversion was obviously decreased, and T_{90} value shifted to higher temperature, which was related to the competitive adsorption of H_2O with CH_2Br_2 molecules at the active sites.

Generally, various organic compounds exist in the Br-VOCs-

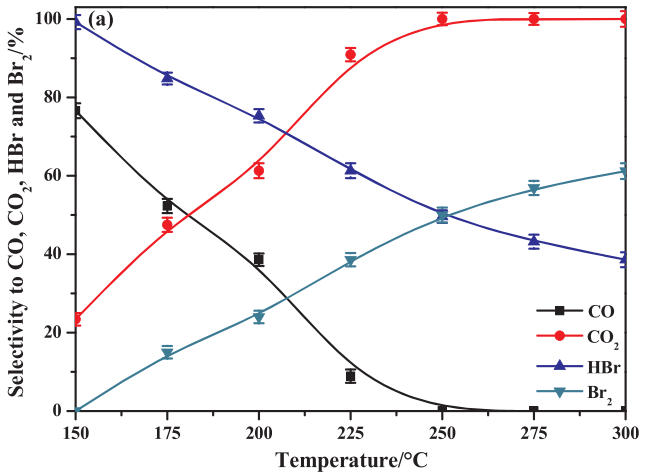

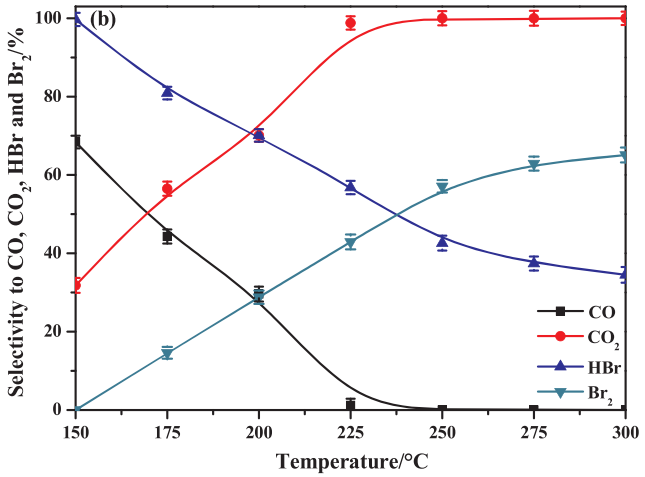

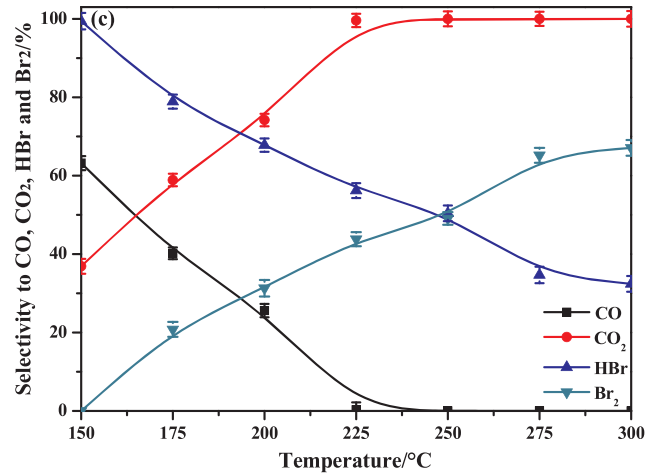

Fig. 7. Selectivity to CO, CO_2, HBr, and Br_2 as a function of temperature over Co_3O_4-B (a), Co_3O_4-S (b), and Co_3O_4-K (c).

containing industrial exhaust gas, but it is unrealistic to simultaneously inspect the influence of various organic compounds on CH_2Br_2 oxidation. Hence, we mainly studied the reaction behaviors touching upon a binary mixture of organic compounds, and CH_2Br_2 conversion over Co_3O_4-K as a function of temperature in the presence of PX as a model PTA-exhaust-gas organic compound is also shown in Fig. 8. When the presence of PX, CH_2Br_2 conversion was remarkably decreased, and T_{90} increased to 294 °C. The depressing influence might be related to the reduction of active sites because of PX oxidation.

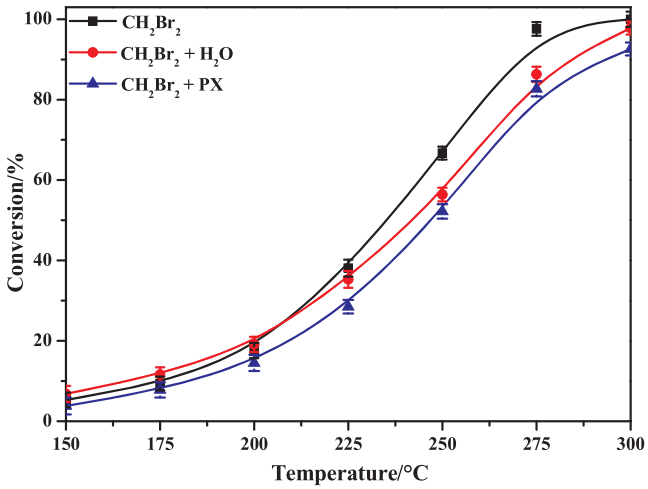

Fig. 8. The influence of H_2O and PX on CH_2Br_2 oxidation over Co_3O_4-K; CH_2Br_2 alone: 500 ppm of CH_2Br_2; CH_2Br_2 + H_2O:500 ppm of CH_2Br_2 + 2% of H_2O; CH_2Br_2 + PX:500 ppm of CH_2Br_2 + 500 ppm of PX; in all cases, 10% of O_2, and the rest being N_2; GHSV = 112,500 $cm^3\,g^{-1}\,h^{-1}$.

3.5. Catalyst stability

For an industrial application, it is essential to investigate the catalyst stability. The stability test was carried out by feeding an air flow comprising 500 ppm of CH_2Br_2, 10% of O_2, and the rest being N_2 at 250 °C with GHSV of 112,500 $cm^3\,g^{-1}\,h^{-1}$, and the results for Co_3O_4-B, Co_3O_4-S, and Co_3O_4-K catalysts are shown in Fig. 9. All the samples displayed highly stable activity for 30 h with CH_2Br_2 conversion of approximately 49, 61, and 66%, respectively. Meanwhile, the positions and intensities of the characteristic peaks corresponding to spinel Co_3O_4 had almost no change after reaction for 30 h, which implied that the structure and composition of the active sites were stable. The deposition of bromine species on the catalyst is often perceived as the primary reason for decrease in activity. XPS analysis shows that the bromine contents de of Co_3O_4-B, Co_3O_4-S, and Co_3O_4-K were 1.07, 1.04, and 1.02%, respectively. The results suggested that ordered mesoporous spinel Co_3O_4 can promote the removal of bromine species from the catalyst surface and enhanced catalyst stability. Stability of Co_3O_4-K for CH_2Br_2 oxidation in the presence of 2% of H_2O or 500 ppm of PX at 250 °C was also investigated (Figure. S2), and the results suggested that Co_3O_4-K could exhibit superior stability for long-term CH_2Br_2 oxidation in the presence of H_2O, and PX, making it potential for industrial application.

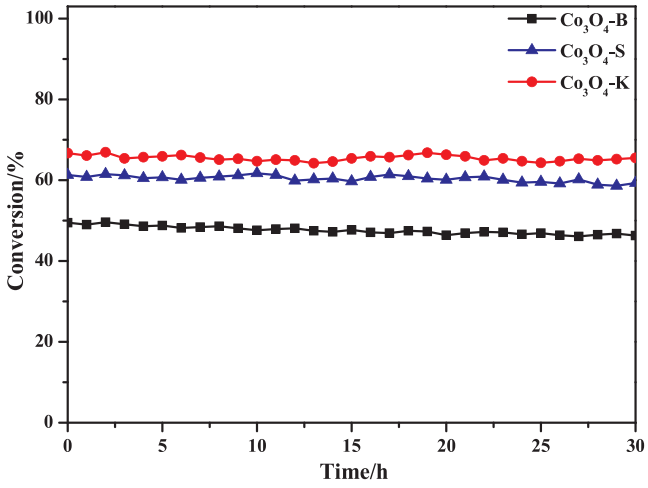

Fig. 9. Stability test of different Co_3O_4 at 250 °C.

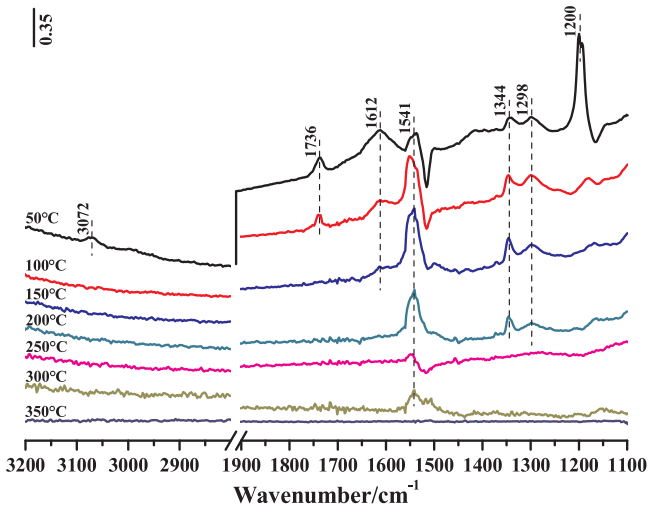

Fig. 10. In situ DRIFT spectra of CH_2Br_2 oxidation over Co_3O_4-K at different temperatures.

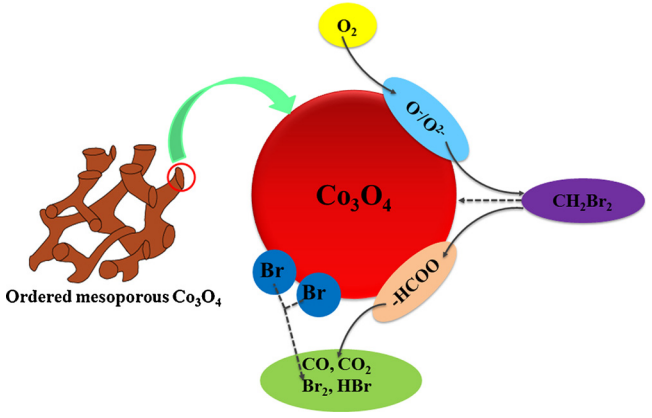

Fig. 11. a reasonable mechanism for CH_2Br_2 oxidation over ordered mesoporous spinel Co_3O_4.

3.6. In situ DRIFT study

To identify the intermediate products generated on the catalyst surface, in situ DRIFT experiments were conducted, and the DRIFT spectra of Co_3O_4-K are shown in Fig. 10 (DRIFT spectra of Co_3O_4-B and Co_3O_4-S are shown in Figure. S3). After treated in a gas flow comprising 500 ppm of CH_2Br_2, 10% of O_2, and the rest being N_2 at 50 °C for 1 h, the bands appeared at 3072, 1736, 1612, 1541, 1344, 1298, and 1200 cm^{-1} were observed. The bands at 3072, and 1200 cm^{-1} were ascribed to asymmetric stretching, and wagging of methylene species, respectively [22]. As the reaction temperature rised up, the bands ascribed to CH_2Br_2 gradually decreased in intensity and disappeared above 100 °C, suggesting either desorption or oxidation of CH_2Br_2 molecules. The band at 1736, and 1612 cm^{-1} was assigned to carbonyl stretching, and H_2O on the catalyst surface, respectively [23,24], they gradually disappeared as the reaction temperature rised up. Meanwhile, the disappearance of the bands related to CH_2Br_2 occurred with the increasing intensities of bands at 1541, 1344, and 1298 cm^{-1}, which were ascribed to asymmetric vibration, symmetric vibration, and −OH deformation vibration of formate species [25]. No bands were observed above 350 °C, which suggest that CH_2Br_2 had been completely oxidized. All the bands generated in the process of CH_2Br_2 oxidation, suggesting that the formate species were the intermediate products on the surface of Co_3O_4-K. Moreover, no bands belonging to CO, CO_2, or HBr were observed due to the quick desorption. Similar spectra were also detected on the Co_3O_4-B, and Co_3O_4-S.

Combined with the results of product analysis, and in situ DRIFT study, a reasonable mechanism for CH_2Br_2 oxidation over ordered mesoporous spinel Co_3O_4 was proposed, and the results are shown in Fig. 11: (1) adsorption of CH_2Br_2 molecules on Co active sites through Br atoms; (2) dissociation of adsorbed CH_2Br_2 through the breakage of C-Br bonds into formate species; (3) adsorption of gas-phase oxygen on the surface to supply the consumed oxygen; (4) formation of CO, and CO_2 through the formate species oxidized by active oxygen species; and (5) the removal of adsorbed Br species from the catalyst surface in the form of Br_2, and HBr.

4. Conclusion

In this work, ordered mesoporous spinel Co_3O_4 were synthesized for the catalytic oxidation of CH_2Br_2 as the model pollutant for Br-VOCs. It is found that ordered mesoporous spinel Co_3O_4 exhibited superior catalytic activity than bulk spinel Co_3O_4. Particularly, Co_3O_4-K showed the highest catalytic activity, and its T_{90} value was only 271 °C. Meanwhile, Co_3O_4-K showed the highest selectivity to CO_2 at low temperature and a good stability for at least 30 h. The superior catalytic activity of ordered mesoporous spinel Co_3O_4 was related to their high specific surface areas, high content of Co^{3+}, and strong redox property. In situ DRIFT study showed that formate species were the main intermediate products generated on the surface of ordered mesoporous spinel Co_3O_4, and a reasonable mechanism for CH_2Br_2 oxidation over ordered mesoporous spinel Co_3O_4 was proposed. Consequently, ordered mesoporous spinel Co_3O_4 can be a promising catalyst for industrial application.

Acknowledgements

This work was supportedby the National Natural Science Fundation of China (No. 51278294), and China's Post-doctoral Science Fun (No. 2017M621484 and 2015M581626).

Appendix A. Supplementary data

Supplementary material related to this article can be found, in the online version, at doi:https://doi.org/10.1016/j.mcat.2018.10.001.

References

[1] H. Dai, S. Jing, H. Wang, Y. Ma, L. Li, W. Song, H. Kan, Sci. Total Environ. 577 (2017) 73–83.
[2] F. Zhang, X. Li, Q. Zhao, D. Zhang, ACS Sustain. Chem. Eng. 4 (2016) 4554–4562.
[3] X. Huang, Environ. Eng. 29 (2011) 97–98.
[4] C.Y. Chen, J.J. Pignatello, Appl. Catal. B 142–143 (2013) 785–794.
[5] X. Liu, J. Zeng, J. Wang, W. Shi, T. Zhu, Catal. Sci. Technol. 6 (2016) 4337–4344.
[6] J. Mei, Y. Ke, Z. Yu, X. Hu, Z. Qu, N. Yan, Chem. Eng. J. 320 (2017) 124–134.
[7] J. Mei, W. Huang, Z. Qu, X. Hu, N. Yan, J. Colloid Interface Sci. 505 (2017) 870–883.
[8] Y.C. Kun Wang, Jindou Hu, Yizhao Li, Jing Xie, Dianzeng Jia, ACS Appl. Mater. Interfaces 9 (19) (2017) 16128–16137.
[9] R. Wang, J.Q. Qi, Y.W. Sui, Y.Z. He, F.X. Wei, Q.K. Meng, Z. Sun, J. Mater. Sci. Mater. Electron. 28 (2017) 9056–9065.
[10] J. Deng, S.F. Feng, K. Zhang, J. Li, H. Wang, T. Zhang, X. Ma, Chem. Eng. J. 308 (2017) 505–515.
[11] H. Tüysüz, J.H. Yun, S.B. Khan, A.M. Asiri, P. Yang, Nano Res. 6 (2013) 47–54.
[12] W. Song, A.S. Poyraz, Y. Meng, Z. Ren, S.Y. Chen, S.L. Suib, Chem. Mater. 26 (2014) 4629–4639.
[13] J. Mei, Z. Qu, S. Zhao, X. Hu, H. Xu, N. Yan, J. Ind. Eng. Chem. 57 (2018) 208–215.
[14] Q. Wang, J. Liu, Y. Li, Z. Zhao, W. Song, Y. Wei, RSC Adv. 7 (2017) 18592–18600.
[15] W. Eom, A. Kim, H. Park, H. Kim, T.H. Han, Adv. Funct. Mater. 26 (2016) 7605–7613.
[16] X. Xie, Y. Li, Z.Q. Liu, M. Haruta, W. Shen, Nature 458 (2009) 746–749.
[17] C. Zhang, L. Zhang, G.C. Xu, X. Ma, Y.H. Li, C. Zhang, D. Jia, New J. Chem. 41 (2017) 1631–1636.
[18] J.-W.S. Zhaoyang Fan, Chen Gao, Ge Gao, Baorui Wang, Chunming Niu, ACS Appl. Mater. Interfaces 9 (2017) 16117–16127.
[19] X. Cao, R. Zhou, N. Rui, Z. Wang, J. Wang, X. Zhou, C.J. Liu, Catal. Today 297 (2017) 219–227.
[20] P.F. Schubert, R.D. Beatty, S. Mahajan, ACS Symp. Ser. (1994) 405–419.
[21] C.E. Hetrick, F. Patcas, M.D. Amiridis, Appl. Catal. B 101 (2011) 622–628.
[22] M.T. Chen, C.F. Lien, A. Lifen Liao, J.L. Lin, J. Phys. Chem. B 107 (2003) 3837–3843.
[23] C.C. Chuang, W.C. Wu, M.C. Huang, I.C. Huang, J.L. Lin, J. Catal. 185 (1999) 423–434.
[24] Y. Wang, A.P. Jia, M.F. Luo, J.Q. Lu, Appl. Catal. B 165 (2015) 477–486.
[25] R. Yang, Y. Fu, Y. Zhang, N. Tsubaki, J. Catal. 228 (2004) 23–35.